



DE82021814

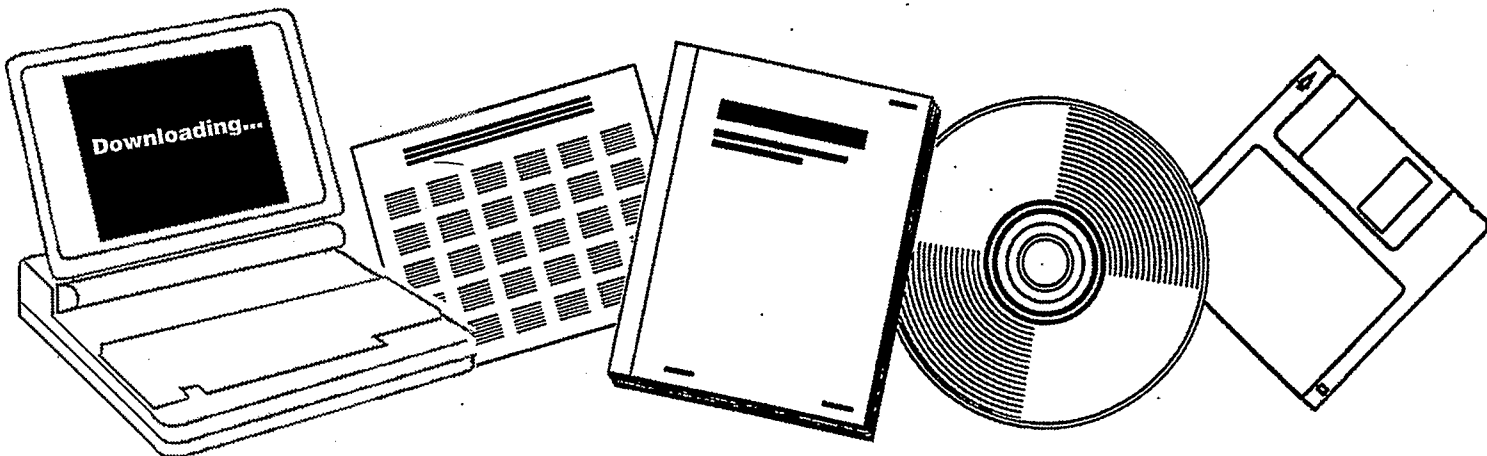
NTIS

One Source. One Search. One Solution.

COLD-FLOW STUDIES FOR THE H-COAL REACTOR. PART II. GAS-MIXING MODEL

AMOCO RESEARCH CENTER
NAPERVILLE, IL

1980



U.S. Department of Commerce
National Technical Information Service



COLD-FLOW STUDIES FOR THE H-COAL REACTOR.
PART II: GAS-MIXING MODEL

I. A. Vasalos, D. N. Rundell, E. M. Bild
Amoco Research Center
Naperville, Illinois 60566

M. H. Peters
Department of Chemical Engineering
The Ohio State University
Columbus, Ohio 43210

MASTER

AC05-77ET10149

ABSTRACT

The gas mixing in a three-phase fluidized bed was studied in a cold flow reactor model. Experiments were conducted using nitrogen, kerosene, and extrudates of hydrodesulfurization catalyst. Utilizing Argon-41 as a tracer, the residence time distribution was studied. Based on these measurements, it was found that addition of coal fines significantly affected the gas flow inside the reactor. It was found that gas bubbles tend to flow upward in the center of the reactor, with a downward flow of gas bubbles near the walls.

SCOPE

The objective of this study was to establish the gas flow characteristics of gas-slurry-catalyst systems in order to obtain a better understanding of the mixing phenomena taking place in the H-Coal reactor. At ambient temperatures, the liquids and fines employed have properties similar to the actual H-Coal reactor fluids. Emphasis in this paper is given to the study of gas flow based on the use of residence time distribution data.

Previous work reported in Part I of this series describes the variation in the average gas holdup with gas and liquid superficial velocities and the

DISCLAIMER

This book was prepared as an account of work sponsored by an agency of the United States Government. Neither the United States Government nor any agency thereof, nor any of their employees, makes any warranty, express or implied, or assumes any legal liability or responsibility for the accuracy, completeness, or usefulness of any information, apparatus, product, or process disclosed, or represents that its use would not infringe privately owned rights. Reference herein to any specific commercial product, process, or service by trade name, trademark, manufacturer, or otherwise, does not necessarily constitute or imply its endorsement, recommendation, or favoring by the United States Government or any agency thereof. The views and opinions of authors expressed herein do not necessarily state or reflect those of the United States Government or any agency thereof.

physical properties of the fluids. This paper extends this work by an attempt to establish the gas holdup by an independent measurement. The use of radioactive tracer gas has been previously considered by Ostergaard and Michelsen. Their work showed that the gas mixing is greatly influenced by the relative gas and liquid velocities and particle size. Their results gave a qualitative picture of gas mixing. The same authors describe the difficulties in utilizing Argon-41 in gas-water-solid systems. Problems caused by the absorption of the tracer by the liquid phase are also compounded by the preferential flow of gas in the center of the reactor. Rigby, et al., reported the tendency of gas to preferentially rise in the center of a gas-liquid fluidized bed. This results in a downward motion of gas at the walls.

CONCLUSIONS AND SIGNIFICANCE

Residence time distribution data with nitrogen, kerosene, and HDS catalyst indicate back-mixing of the gas phase. This becomes even more pronounced with addition of coal fines at a concentration of 15.5 vol%. Using standard mathematical techniques to calculate first and second moments, the Peclet numbers were derived. Values ranged from 5 to 0.7 without and with fines, respectively. Calculation of an apparent linear velocity was used to derive average gas holdup in the catalyst bed. A comparison of the latter with values reported using the gamma-ray technique (Part I) shows significant differences. It is believed that the lower holdup values calculated from the tracer tests are the result of gas back-mixing. A two-flow-regime model is proposed to describe the gas flow. Large bubble coalesce and rise through the reactor center, and a downward stream of gas flows near the reactor

walls. Each flow regime is composed of series of completely mixed tanks. The model parameters were obtained to best fit the experimental data. The variation of parameters with operating conditions is discussed.

INTRODUCTION

It was reported in Part I that there is a need to study the complex mixing behavior in the H-Coal reactor under controlled operating conditions. In the work described earlier (Vasalos, et al., 1980), extrudates of hydrogenation catalyst were fluidized with coal char-kerosene slurries and nitrogen. Main emphasis was placed on determining the catalyst holdup, while the gas holdup was determined indirectly.

Another possible technique for the direct measurement of gas holdup is with the use of radioactive gas tracers. With this technique, the residence time of the tracer along the reactor is monitored with externally mounted scintillation crystal detectors. Thus, no flow disturbance is caused.

The use of radioactive gas tracer tests in a three-phase system was previously reported by Michelsen (1970). In a bed of glass particles fluidized with water and nitrogen, radioactive gas was injected and monitored by two external detectors. Results were used to give a qualitative description of gas mixing. Ostergaard (1969) presented a preferred method of analysis of tracer data from a mathematical, imperfect injection. It is the objective of this paper to compare gas holdups computed directly from gas tracers with those calculated indirectly from either the gamma-ray scan technique or differential

pressure transmitters. Based on the results of this comparison, a gas mixing model is proposed.

EXPERIMENTAL

As discussed previously (Vasalos, et al., 1980), the equipment used for this study is almost on scale with the 3 t/d coal liquefaction process development unit (PDU) operated by Hydrocarbon Research, Incorporated. The reactor vessel used in the cold flow studies is a 15.2 cm ID vessel, 6 m in length. It is constructed from four glass sections connected by metal spool pieces having entries for sample taps, pressure taps, and thermowells.

Experimental techniques for determining the catalyst holdup were described in Part I. In this paper, emphasis is given on analyzing gas residence time distribution data in a gas-liquid-solid fluidized bed composed of extrudates of desulfurization catalyst 1.8 mm in diameter and 5.1 mm in length. Data are presented with nitrogen-kerosene and nitrogen-slurry made of 15.5 vol% coal char in kerosene. Properties of these fluids and solids have been reported in Part I.

The Argon-41 isotope used in this study was prepared by the high neutron flux bombardment of Argon-40. Because Argon-41 has a half-life of 1.8 hours, the gas tracer tests must be carried out with a strict time schedule to insure at least 150 mc at the start of each test.

The tracer was injected through a tube inserted into the reactor above the bubble cap distributor. Michelsen and Ostergaard (1970) noted difficulties in analyzing tracer data due to the interphase transfer of argon. Therefore, non-radioactive A^{40} was used to presaturate the system before injection of the tracer. Experiments also showed that absorption of argon by coal fines is negligible.

Six scintillation detectors were mounted on the system as shown in Figure 1. The spacing between detectors is shown in the same figure. Detectors 1 and 2 always viewed the catalyst bed. Detectors 3 and 4 always viewed the liquid or slurry phase above the bed. Detectors 5 and 6 viewed gas lines only, and were used primarily to estimate the overall gas holdup in the system.

Each detector consists of a sodium iodide crystal optically interfaced with photomultiplier tubes, which are supplied with a constant voltage of 1500 volts. Pulse height analyzers used in conjunction with a linear rotameter insure the detection of particles which lie within a desired energy range. Argon-41 decays by emitting particles with energies of 1.3 MeV. The instrument is adjusted to count particles with energies from 1.3 MeV down to a level high enough to screen out the background radiation. High collimation of all detectors with lead shielding permitted a view of a thin, vertical segment of the entire reactor cross-section.

The detection system included a high-speed data recorder and a data acquisition system linked to a ModComp II mini computer. The data were collected at two rates---either 5 or 10 measurements per second.

Tracer Data Analysis

In analyzing tracer data, it is first assumed that the flow of gas phase may be described by the axially dispersed piston flow model. An axial dispersion coefficient can be calculated when two parameters are found from the residence time distribution of a pulse injected in a flow system: the first moment (μ) and the second moment (σ^2). The first moment is related to the mean residence time (τ) monitored between two reactor locations by the following equation:

$$\tau = \mu_2 - \mu_1 \quad (1)$$

The first and second moments are determined from the following equations:

$$\mu = \frac{\int_0^{\infty} t c(t) dt}{\int_0^{\infty} c(t) dt} \quad (2)$$

$$\sigma^2 = \frac{\int_0^{\infty} t^2 c(t) dt}{\int_0^{\infty} c(t) dt} - \mu^2 \quad (3)$$

The integrals appearing in Equations 2 and 3 were evaluated on the computer numerically using standard procedures. Error due to the numerical procedure should be minimal because of the very small (less than 0.2 sec) interval size used. However, calculation of moments using Equations 2 and 3 can result in significant errors due to low concentration values at long times (Ostergaard, 1969). This error can be minimized by using a modified method of analysis of moments. This method utilizes a Laplace transform of a concentration distribution:

$$c(s) = \frac{\int_0^{\infty} c(t) \exp(-st) dt}{\int_0^{\infty} c(t) dt} \quad (4)$$

Differentiating with respect to s gives:

$$\frac{d^n}{ds^n}(c(s)) = -1^n \int_0^{\infty} t^n c(t) \exp(-st) dt / \int_0^{\infty} c(t) dt \quad (5)$$

The modified first moment is found by calculating the slope of a plot of $c(s)$ versus s as s approaches zero. The second moment is determined in a similar fashion.

Both methods were used to calculate the moments of the gas tracer concentration/time curves. The difference in the moments evaluated by the two different methods is an indication of the error in the concentration distribution at long times.

A comparison of first and second moments calculated first by Equations 2 and 3 and second by the modified method of analysis of moments is given in Table I. Agreement between the two methods of calculations is excellent, suggesting that errors introduced by using Equations 2 and 3 are minimal.

The gas linear velocity (V_g) between Locations 1 and 2 can be determined from the first moments by the following equation:

$$V_g = \frac{h}{\mu_2 - \mu_1} \quad (6)$$

where h is the distance between Locations 1 and 2.

In addition, both first and second moments can be used to estimate parameters of an axial dispersion piston flow model. Mixing of the gas in the system studied is characterized by the Peclet number:

$$\frac{1}{Pe_g} = \frac{E_g}{V_g h} \quad (7)$$

where E_g is the dispersion coefficient.

A simple relation between moments and the dispersion coefficient was given by Aris (1959) as:

$$\frac{\Delta\sigma^2}{(\Delta\mu)^2} = \frac{2E_g}{V_g h} \quad (8)$$

RESULTS AND DISCUSSION

Residence time distribution curves obtained from gas tracers can be used to calculate the gas holdup in the reactor if it is assumed that the flow of the gas can be characterized by a constant linear velocity (V_g):

$$\epsilon_g = U_g / V_g \quad (9)$$

Typical residence time distribution data without and with (15.5 vol%) coal char fines are shown in Figures 2 and 3, respectively. The residence time distribution is significantly different from the one expected for either plug flow or completely mixed ideal reactors (Levenspiel). In the present case it is expected that the detector's finite view has an effect on the time

distribution curves. This is because, in spite of the high collimation, the detector will sense the isotope before the tracer is actually directly in front of the detector crystal.

As seen in Figures 2 and 3, the distribution curves are skewed positive with increasing time, indicating the the reactor has significant back-mixing (Levenspiel). This becomes even more pronounced with addition of coal fines, which results in a more rapid tracer response at the top of the bed, combined with increased dispersion and apparent back-mixing. These results support conclusions reported previously (Vasalos, 1980) that addition of coal fines enhances bubble coalescence, causing the formation of larger bubbles which rise quickly through the reactor.

To quantify the extent of gas mixing inside the reactor, Equations 7 and 8 were used to calculate the gas dispersion coefficients inside the bed (Detectors 1 and 2) and the region above the catalyst bed (Detectors 3 and 4). These results are reported in Table IV. From the magnitude of the dispersion coefficients, it is confirmed that there is apparent gas back-mixing throughout the reactor.

The gas linear velocity in the catalyst bed and above the catalyst (dilute phase) was calculated from the tracer results for several cases. The calculated velocities and test conditions are shown in Table II. Replicates for each case show generally good agreement. Comparison of gas velocities with and without coal fines at similar operating conditions shows that the average gas velocity in the catalyst bed is not significantly changed.

A comparison of gas holdup calculated from gamma-ray scans with tracer results is shown in Table III. In all cases, the values calculated from tracer results are significantly higher than those determined from gamma-ray scans. As discussed earlier, results from the tracer test reflect the gas holdup in the entire reactor cross-section, whereas the gas holdup calculated from gamma-ray scans reflects a value corresponding to a measurement taken across the diameter of the reactor.

To determine if a radial gas distribution could account for the difference between holdups calculated by the two methods, gamma-ray scans through three chords of the reactor were obtained. Gas holdups were determined through the reactor center and on two chords at different conditions.

In general, the results were all within experimental error. This implies there is not a significant radial distribution of gas which could account for the large differences between holdups calculated by the two techniques.

It is believed that the discrepancy in the calculated holdups can be explained by the gas flow pattern inside a reactor. Flow of large gas bubbles in the center of the reactor followed by downward flow of gas near the walls will result in long residence time distributions. This in turn will give apparently low linear gas velocities and high gas holdups. On the other hand, the gas holdup calculated from other techniques is independent of the direction in the gas flow.

Rigby, et al., also reported the tendency of gas bubbles to preferentially rise in the center of a gas-liquid fluidized bed. This results in a downward motion of gas at the walls which may cause the spreading of the tracer concentration, as indicated by the comparison of the second moments for Tests 1 and 2. This comparison indicates that coal fines cause the tracer to spread out in the reactor, possibly as a result of the downflow of gas near the walls.

The qualitative picture of large bubbles traveling up in the center of the reactor causing downflow at the walls is consistent with the differences in holdups calculated by the two methods. Visual observation of the reactor also supports this model. A significant downflow of small gas bubbles can be seen at the reactor walls.

Results from the gamma-ray scans through different chords of a horizontal section are also consistent with this model for gas flow in the reactor. The gas holdup in the two different flow regimes could be the same, although the gas is traveling in different directions.

The ratio between the gas holdups calculated from gas tracer and gamma-ray tests can be related to the amount of gas in each flow regime. However, it must be assumed that the detector views the reactor impartially; tracer in the center of the reactor contributes equally to the total signal to the tracer at the walls. As the ratio of tracer to gamma-ray scan calculated gas holdups increases, the fraction of gas traveling down in the reactor or the cross-sectional area occupied by gas moving down increases. This ratio

increases with the addition of coal fines to the reactor, supporting previous indications that coal fines enhance bubble coalescence to form large bubbles which would rise through the center of the reactor. Because of these flow characteristics, the model presented in the next section is proposed.

Gas Mixing Model

In order to describe the bubble flow behavior of gas and the various degrees of gas mixing which may occur in each region, a circulation model consisting of n and m completely mixed tanks is proposed. This is shown schematically in Figure 4. The solution to the exit age distribution function for the system is also shown in Figure 4, is somewhat complex, but has been obtained by a stepwise procedure (Appendix A). The result in dimensionless form may be written as:

$$E(\theta) = \left(\frac{E}{1 + \lambda} \right) \sum_{R=1}^{R^*} \left\{ \left(\frac{\lambda}{1 + \lambda} \right)^{R-1} \frac{1}{t_1^a t_2^b} \left[e^{-\tau_1 \theta} \right. \right. \quad (10)$$

$$\left. \sum_{r=1}^a \frac{1}{(r-1)!} \frac{d^{r-1}}{ds^{r-1}} [(S - a_1)^a f(S)] \Big|_{S = a_1} \cdot \frac{t^{a-r}}{(a-r)!} \right.$$

$$+ e^{-\tau_2 \theta} \sum_{r=1}^b \frac{1}{(r-1)!} \frac{d^{r-1}}{ds^{r-1}} [(S - a_2)^b f(S)] \Big|_{S = a_2} \cdot \left. \frac{t^{b-r}}{(b-r)!} \right\}$$

Note that for R = 1, Equation 10 will collapse to:

$$E(\theta) = \frac{V}{V_1} \frac{\bar{\tau}}{\tau_1^n} \frac{\tau_1^{n-1}}{(n-1)!} e^{-t/\tau_1} \quad (11)$$

which is the response of n CSTR's in series (Himmeiblauf, et al.), modified for a volume fraction of less than one.

Figure 5 shows the flow diagram for the computational procedures based on the proposed model. Calculations of the exit age distribution function begin with specifications of n , m , λ , and P_1 . Assuming that the n tanks are all of equal size, V_n/n , and that the m tanks are all of equal size, V_m/m , the following relationships can be easily shown to hold:

$$\frac{\bar{\tau}_1}{\bar{\tau}_2} = \frac{P_1}{P_2} \left(\frac{m}{n} \right) \left(\frac{\lambda}{1 + \lambda} \right)$$

$$\bar{\tau} = \bar{\tau}_1 n (1 + \lambda) + \bar{\tau}_2 m \lambda \quad (12)$$

where: $P_1 = V_n/V$
 $P_2 = V_m/V$
 $P_2 = 1 - P_1$

The exit age distribution is calculated from Equation 10, and the appropriate recursion formula from the derivatives (Appendix A). It should be noted that the mathematical techniques employed in the present model development have been found to yield identical results with those given by Mann, et al.

Figures 6 and 7 show some typical response curves obtained from the model. For most regions of interest, the initial response of such a system is controlled by the number of tanks in the upflow stream and the upflow volume fraction. The influence of the recycle branch will largely affect the later decay of the response signal.

Application to Experimental Radiotracer Data

The present model may be employed to describe flow patterns observed during the radiotracer tests. Figure 8 shows a typical result obtained by best fit of the parameters of the present model for the case of no coal fines in kerosene. In this case, the degree of mixing was always found to be intermediate between complete mixing and plug flow, as indicated in Figure 8. The recycle flow was found to be about 10% of the total flow, which was qualitatively verified by visual observations.

The addition of fines to the kerosene changed the residence time distribution as indicated in Figure 9. For the two experiments shown, the behavior is closely represented by one completely mixed reactor with a small recycle flow, as in Figure 9. The apparent time delay of 0.2θ (corresponding to 2-3 seconds) may be related to the rise time for a large gas bubble. The present model predictions of increased gas mixing due to the addition of coal fines is qualitatively consistent with the previous finding of a transition to churn turbulent flow.

APPENDIX A

MATHEMATICAL DEVELOPMENT OF GAS MIXING MODEL

Gas flow in three-phase systems described previously has been shown to be generally characterized by an upflow of gas bubbles in the center region of the bed and a downflow of gas bubbles near the wall region. In order to describe the various degrees of gas mixing which may occur in each region, a circulation model consisting of n and m completely mixed tanks is proposed. This is shown schematically in Figure 4.

A material balance at the node where the recirculation stream and input stream meet leads to the equation

$$vC_1 + v_2C_2 = v_1C_1 \quad (A-1)$$

To derive the response equation to the system shown in Figure 4, consider the transfer function in the Laplace domain for the n and m tanks, respectively (Wen and Fan, 1975):

$$\frac{C_0(S)}{C_1(S)} = \frac{1}{[S \frac{V_n}{nv_1} + 1]^n} \quad (A-2)$$

$$\frac{C_2(S)}{C_0(S)} = \frac{1}{[S \frac{V_m}{mv_2} + 1]^m} \quad (A-3)$$

Taking the Laplace transform of Equation A-1 and rearranging gives

$$\frac{v}{v_1} C_1(S) + \frac{v_2}{v_1} C_2(S) = C_1(S) \quad (A-4)$$

Substituting the transfer functions into Equation A-4 and rearranging gives

$$\frac{C_o(S)}{C_1(S)} = \frac{\frac{v}{v_1} [S\bar{t}_2 + 1]^m}{\{[S\bar{t}_1 + 1]^n [S\bar{t}_2 + 1]^m - \frac{v_2}{v_1}\}} \quad (A-5)$$

where $\bar{t}_1 = V_n/nv_1$ and $\bar{t}_2 = V_m/mv_2$, assuming equal sized tanks in each stream.

Letting $A = v/(v_1\bar{t}_1^n)$ and $B = v_2/v_1(1/\bar{t}_1^n\bar{t}_2^m)$ gives a more workable form of Equation A-5 as

$$\frac{C_o(S)}{C_1(S)} = \frac{A(S + 1/\bar{t}_2)^m}{[(S + 1/\bar{t}_1)^n (S + 1/\bar{t}_2)^m - B]} \quad (A-6)$$

Equation A-6 is the general transfer function for the recirculation model shown in Figure 4.

Consider now the analytical response equation of the system to an impulse input of tracer.

The first output signal will be for the n tanks alone--i.e., $C_2(S) = 0$

$$C_2(S) = \frac{v}{v_1} C_1(S) \quad (A-7)$$

$$\frac{C_o(S)}{C_1(S)} = \frac{1}{(S\bar{t}_1 + 1)^n} \quad (A-8)$$

Substituting Equation A-7 into Equation A-8 gives the transfer function for the first output signal as

$$\frac{C_0(S)}{C_1(S)} = \frac{v/v_1}{(s\bar{t}_1 + 1)^n} \quad (A-9)$$

The second output signal, corresponding to one complete loop, may be obtained by first substituting Equation A-9 into Equation A-3

$$\frac{C_2(S)}{C_1(S)} = \frac{v/v_1}{(s\bar{t}_1 + 1)^n} \left\{ \frac{1}{(s\bar{t}_2 + 1)^m} \right\} \quad (A-10)$$

A material balance at the first node gives $C_1(S) = 0$

$$C_1(S) = \frac{v_2}{v_1} C_2(S) \quad (A-11)$$

Substituting Equation A-11 into Equation A-10

$$\frac{C_1(S)}{C_1(S)} = \frac{v/v_1}{(s\bar{t}_1 + 1)^n} \left\{ \frac{v_2/v_1}{(s\bar{t}_2 + 1)^m} \right\} \quad (A-12)$$

Substituting Equation A-12 into Equation A-2 yields the transfer function for one complete loop as

$$\frac{C_0(S)}{C_1(S)} = \frac{v/v_1}{(s\bar{t}_1 + 1)^n} \left\{ \frac{v_2}{v_1} \frac{1}{(s\bar{t}_2 + 1)^m} \frac{1}{(s\bar{t}_1 + 1)^n} \right\} \quad (A-13)$$

Continuing this procedure, it can easily be shown that the overall transfer function with an impulse input to the system may be generally written

$$\frac{C_o(S)}{C_i(S)} = \frac{v}{v_1} \sum_{R=1}^{R^*} \left\{ \left(\frac{v_2}{v_1} \right)^{R-1} \frac{1}{(S\bar{t}_1 + 1)^{Rn}} \frac{1}{(S\bar{t}_2 + 1)^{(R-1)m}} \right\} \quad (A-14)$$

Letting $a = Rn$ and $b = (R-1)m$

$$\frac{C_o(S)}{C_i(S)} = \frac{v}{v_1} \sum_{R=1}^{R^*} \left\{ \left(\frac{v_2}{v_1} \right)^{R-1} \frac{1}{\bar{t}_1^a \bar{t}_2^b} \frac{1}{(S + 1/\bar{t}_1)^a (S + 1/\bar{t}_2)^b} \right\} \quad (A-15)$$

In order to obtain the inverse function, first consider the term

$$\frac{1}{(S - a_1)^a (S - a_2)^b}$$

where $a_1 = -1/\bar{t}_1$

and $a_2 = -1/\bar{t}_2$

Now consider a Heaviside expansion formula for repeated roots (Bronwell, 1953)

$$\begin{aligned} f(S) &= \frac{1}{(S - a_1)^a (S - a_2)^b} \\ &= \frac{A_1}{(S - a_1)^a} + \frac{A_2}{(S - a_1)^{a-1}} + \dots + \frac{A_a}{(S - a_1)} \\ &+ \frac{C_1}{(S - a_2)^b} + \frac{C_2}{(S - a_2)^{b-1}} + \dots + \frac{C_b}{(S - a_2)} \\ &= \sum_{r=1}^a \frac{A_r}{(S - a_1)^{a-r+1}} + \sum_{r=1}^b \frac{C_r}{(S - a_2)^{b-r+1}} \end{aligned} \quad (A-16)$$

In order to obtain the values of the coefficients, first multiply both sides of Equation A-16 by $(S - a_1)^a$

$$f(S)(S - a_1)^a = A_1 + A_2(S - a_1) + \dots + A_a(S - a_1)^{a-1} + (S - a_1)^a \left\{ \sum_{r=1}^b \frac{C_r}{(S - a_2)^{b-r+1}} \right\}$$

or:

$$f(S)(S - a_1)^a = \sum_{r=1}^a (S - a_1)^{r-1} A_r + (S - a_1)^a h_1(S) \tag{A-17}$$

$$\text{where } h_1(S) = \sum_{r=1}^b \frac{C_r}{(S - a_2)^{b-r+1}}$$

Differentiating Equation A-17 successively $(M - 1)$ times, where $1 \leq M \leq a$, all terms in the summation from $r = 1$ to $r = M - 1$ disappear, leaving

$$\frac{d^{M-1}}{ds^{M-1}} [(S - a_1)^a f(S)] = \sum_{r=M}^a (r - 1)(r - 2) \dots (r - M + 1) \left[(S - a_1)^{r-M} A_r \right] + \frac{d^{M-1}}{ds^{M-1}} (S - a_1)^a h_1(S)$$

Setting $S = a_1$, all terms will disappear except that in which $r = M$. In the remaining term, replace M by r

$$A_r = \frac{1}{(r - 1)!} \frac{d^{r-1}}{ds^{r-1}} [(S - a_1)^a f(S)] \Big|_{S = a_1} \tag{A-18}$$

where $1 \leq r \leq a$.

The coefficients C_r can be determined in a similar fashion as

$$C_r = \frac{1}{(r-1)!} \frac{d^{r-1}}{ds^{r-1}} [(s-a_2)^b f(s)] \Big|_{s=a_2} \quad (A-19)$$

where $1 \leq r \leq b$.

Making use of the Laplace transform pairs

$$\mathcal{L}^{-1} \left\{ \frac{1}{(s-a_1)^k} \right\} = \frac{t^{k-1}}{(k-1)!} e^{a_1 t}$$

$$\mathcal{L}^{-1} \{f_1(s) + f_2(s)\} = \mathcal{L}^{-1} \{f_1(s)\} + \mathcal{L}^{-1} \{f_2(s)\} = f_1(t) + f_2(t)$$

Leads to

$$f(t) = \sum_{r=1}^a A_r \frac{t^{a-r}}{(a-r)!} e^{a_1 t} + \sum_{r=1}^b C_r \frac{t^{b-r}}{(b-r)!} e^{a_2 t}$$

Substituting Equations A-18 and A-19 into the above gives

$$f(t) = e^{a_1 t} \sum_{r=1}^a \frac{1}{(r-1)!} \frac{d^{r-1}}{ds^{r-1}} [(s-a_1)^a f(s)] \Big|_{s=a_1} \cdot \frac{t^{a-r}}{(a-r)!} \\ + e^{a_2 t} \sum_{r=1}^b \frac{1}{(r-1)!} \frac{d^{r-1}}{ds^{r-1}} [(s-a_2)^b f(s)] \Big|_{s=a_2} \cdot \frac{t^{b-r}}{(b-r)!}$$

The dimensionless exit age distribution function may now be obtained from the inverse of Equation A-15 and by noting that $E(\theta) = \bar{t}E(t)$.

$$\begin{aligned}
 E(\theta) = & \frac{\sqrt{t}}{\sqrt{t}} \sum_{R=1}^{R^*} \left\{ \left(\frac{\sqrt{t}}{\sqrt{t}} \right)^{R-1} \frac{1}{t_1^a t_2^b} \left[e^{a_1 t} \sum_{r=1}^a \frac{1}{(r-1)!} \frac{d^{r-1}}{ds^{r-1}} \right. \right. \\
 & [(s - a_1)^a f(s)] \Big|_{s=a_1} \cdot \frac{t^{a-r}}{(a-r)!} + e^{a_2 t} \sum_{r=1}^b \frac{1}{(r-1)!} \frac{d^{r-1}}{ds^{r-1}} \\
 & \left. \left. [(s - a_2)^b f(s)] \Big|_{s=a_2} \cdot \frac{t^{b-r}}{(b-r)!} \right] \right\} \quad (A-20)
 \end{aligned}$$

$$\begin{aligned}
 E(\theta) = & \left(\frac{E}{1+\lambda} \right) \sum_{R=1}^{R^*} \left\{ \left(\frac{\lambda}{1+\lambda} \right)^{R-1} \frac{1}{t_1^a t_2^b} \left[e^{-\tau_1 \theta} \right. \right. \\
 & \sum_{r=1}^a \frac{1}{(r-1)!} \frac{d^{r-1}}{ds^{r-1}} [(s - a_1)^a f(s)] \Big|_{s=a_1} \cdot \frac{t^{a-r}}{(a-r)!} \\
 & + e^{-\tau_2 \theta} \sum_{r=1}^b \frac{1}{(r-1)!} \frac{d^{r-1}}{ds^{r-1}} [(s - a_2)^b f(s)] \Big|_{s=a_2} \cdot \\
 & \left. \left. \frac{t^{b-r}}{(b-r)!} \right] \right\} \quad (A-21)
 \end{aligned}$$

Generalized recursion formulas for the derivative terms may be readily derived as

$$\begin{aligned}
 & \frac{d^{r-1}}{ds^{r-1}} \left[\frac{1}{(s - a_2)^b} \right] \Big|_{s=a_1} \quad (A-22) \\
 = & \frac{(-b)[- (b+1)][- (b+2)] \dots [- (b+r-2)]}{(a_1 - a_2)^{b+r-1}} \text{ for } r > 1.
 \end{aligned}$$

and

$$\begin{aligned}
 & \frac{d^{r-1}}{ds^{r-1}} \left[\frac{1}{(s - a_1)^a} \right] \Big|_{s=a_2} \\
 = & \frac{(-a)[- (a+1)][- (a+2)] \dots [- (a+r-2)]}{(a_2 - a_1)^{a+r-1}} \text{ for } r > 1. \quad (A-23)
 \end{aligned}$$

NOMENCLATURE

a	Rn
a_1	$-1/\bar{t}_1$
a_2	$-1/\bar{t}_2$
A	$v/(v_1 \bar{t}_1^n)$
A_r	First term coefficients in partial fraction expansion
b	$(R-1)m$
B	$(v_2/v_1)(1/\bar{t}_1^n \bar{t}_2^m)$
C	Outlet tracer concentration from system (arbitrary units)
C_1	Inlet tracer concentration to the n tanks (arbitrary units)
C_2	Second term coefficients in partial fraction expansion
$c(s)$	Concentration function in the Laplace domain
$c(t)$	Concentration function in the time domain
E_g	Dispersion coefficient
$E(t)$	Exit age distribution function (1/time)
$E(\theta)$	Dimensionless exit age distribution function
h	Distance between detectors
m	Number of tanks in downflow region
n	Number of tanks in upflow region
Pe	Peclet number
R	Output signal number
R^*	Maximum number of cycles
\bar{t}	Mean residence time, seconds
\bar{t}_1	Mean residence time in the nth tank
\bar{t}_2	Mean residence time in the mth tank

(Continued)

NOMENCLATURE

U_g	Superficial gas velocity, cm/sec
U_l	Superficial liquid velocity, cm/sec
\dot{V}_g	Linear gas velocity, cm/sec
V	Total gas volumetric flow rate
V_1	Gas volumetric flow rate in upflow stream
V_2	Gas volumetric flow rate in downflow stream
v	Total gas volume in system
V_m	Total volume of the m tanks
V_n	Total volume of the n tanks

Greek

ϵ	Bed voidage
ϵ_g	Volume fraction of gas
ϵ_{p1}	Volume fraction in upflow stream
ϵ_{p2}	Volume fraction in downflow stream
θ	Dimensionless time
$\bar{\theta}_p$	Initial delay in plug flow element
λ	Recycle ratio
μ	First moment
σ_n^2	Second moment, sec

REFERENCES

Aris, R., Chem Eng Sci, 9, 266, 1959

Bhatia, V. K., and N. Epstein, "Three-Phase Fluidization. A Generalized Wake Model," Proc Euro Symp on Fluidiz, p 380, 1974.

Bronwell, A., Advanced Mathematics in Physics and Engineering, McGraw Hill, New York (1953).

Calderbank, P. H., et al., "Coalescence in Bubble Reactors and Absorbers," Third Euro Symp on Chem React Eng, No. 43, p 91, 1964.

Himmelblau, D. M., and K. B. Bischoff, Process Analysis and Simulation Deterministic Systems, John Wiley and Sons, New York (1968).

Levenspiel, O., Chemical Reaction Engineering, Second Edition, John Wiley and Sons, New York (1972).

Mann, V., et al., "Characterization and Analysis of Continuous Recycle Systems," AIChE Journal, 25, 873, 1979.

Massimila, L., et al., "Gas Dispersion in Solid-Liquid Fluidized Beds," Br Chem Eng, Vol 6, p 232 (1961).

McCracken, D. D., Fortran with Engineering Applications, John Wiley and Sons, New York (1967).

Michelsen, M. L., and K. Ostergaard, "Holdup and Fluid Mixing in Gas-Liquid Fluidized Beds," Chem Eng Journal, Vol 1, p 37, 1970.

Ostergaard, K., and M. L. Michelsen, "Holdup and Axial Dispersion in Gas-Liquid Fluidized Beds," AIChE-IIQPR Meeting, Tampa, Florida, May 19-22, 1968.

Ostergaard, K., and P. I. Theisen, "The Effect of Particle Size and Bed Height on the Expansion of Mixed Phase (Gas-Liquid) Fluidized Beds," Chem Eng Sci, Vol 21, pp 413-417, 1966.

Ostergaard, K., and M. L. Michelsen, "On the Use of the Imperfect Tracer Pulse Method for Determination of Holdup and Axial Mixing," Can. J of Chem Eng, Vol 47, pp 107-112, April, 1969.

Rigby, G. R., et al., "Properties of Bubbles in Three-Phase Fluidized Beds as Measured by an Electroresistivity Probe," Chem Eng Sci, Vol 25, pp 1729-1741, 1970.

Stewart, P. S. B., and J. F. Davidson, "Three-Phase Fluidization: Water, Particles, and Air," Chem Eng Sci, Vol 19, pp 319-322, 1964.

Vasalos, I. A., et al., "Study of Ebullated Bed Fluid Dynamics for H-Coal," Final Report, Contract No. DE-AC05-77ET-10149, February, 1980.

Vasalos, I. A., et al., "Experimental Techniques for Studying the Fluid Dynamics of the H-Coal Reactor," Coal Processing Technology, Vol VI, 1980.

Wen, C. Y., and L. T. Fan, Models for Flow Systems and Chemical Reactors, Marcel Dekker, Inc., New York (1975).

TABLE I

FIRST AND SECOND MOMENTS CALCULATED BY TWO METHODS

<u>Test</u>	<u>Detector</u>	<u>m (1)</u> <u>Sec</u>	<u>mm (1)</u> <u>Sec</u>	<u>m (2)</u> <u>Sec²</u>	<u>mm (2)</u> <u>Sec²</u>
1a	1	--	--		
	2	22.9	22.9	117	120
	3	47.6	47.5	785	786
	4	75.7	74.4	1170	1300
	5	90.5	90.0	1502	1600
2a	1	19.6	19.5	--	850
	2	25.2	25.1	1088	1100
	3	48.6	48.4	2184	2160
	4	78.4	77.4	3040	3048
	5	95.2	95.0	3860	3900
3a	1	14.8	14.8	94.8	95.0
	2	24.2	24.2	394	380
	3	53.8	53.4	2560	2520
	4	69.6	69.0	2604	2608
	5	73.2	72.6	2632	2636

m (1), m (2): Moments calculated using Equations 2 and 3.

mm (1), mm (2): Moments calculated using the modified method.

TABLE II

CALCULATED GAS LINEAR VELOCITIES

Kerosene, Nitrogen, American Cyanamid
HDS-2A Catalyst, l = 4.8 mm, d = 1.6 mm

Test	U ₁ , cm/sec	U _g , cm/sec	Vol% Fines	Tracer		Gamma-Ray	
				V _g in Bed cm/sec	V _g Above Bed cm/sec	V _g in Bed cm/sec	V _g Above Bed cm/sec
1a	3.0	3.0	0	13.6	5.6	15.8	12.5
1b	3.0	3.0	0	11.9	5.6	15.8	12.5
2a	3.0	3.0	15.5	14.1	6.2	21.4	25.0
2b	3.0	3.0	15.5	9.8	5.5	21.4	25.0
3a	3.0	4.6	15.5	14.8	10.0	35.3	30.7
3b	3.0	4.6	15.5	14.8	9.5	35.3	30.7

TABLE III
GAS HOLDUPS CALCULATED FROM GAS TRACER
AND GAMMA-RAY TESTS

<u>Test</u>	<u>U₁, cm/sec</u>	<u>U_g, cm/sec</u>	<u>Vol% Fines</u>	<u>Tracer</u>		<u>Gamma-Ray</u>	
				<u>In Bed</u>	<u>Above Bed</u>	<u>In Bed</u>	<u>Above Bed</u>
1a	3.0	3.0	0	0.22	0.54	0.19	0.24
2a	3.0	3.0	15.5	0.22	0.49	0.14	0.12
3a	3.0	4.6	15.5	0.31	0.46	0.13	0.15

TABLE IV

CALCULATION OF DISPERSION COEFFICIENT

<u>Test</u>	<u>Detectors</u>	<u>Gas Velocity, cm/sec</u>	<u>P_e</u>	<u>E_g*</u>
1a	1-2	13.6	5.1	492
	3-4	5.6	3.4	260
2a	1-2	14.1	0.78	3354
	3-4	6.2	2.39	408
3b	1-2	14.8	1.40	1960
	3-4	9.5	1.65	910

*E_g in sec/cm².

Figure 1

Radiotracer detector location

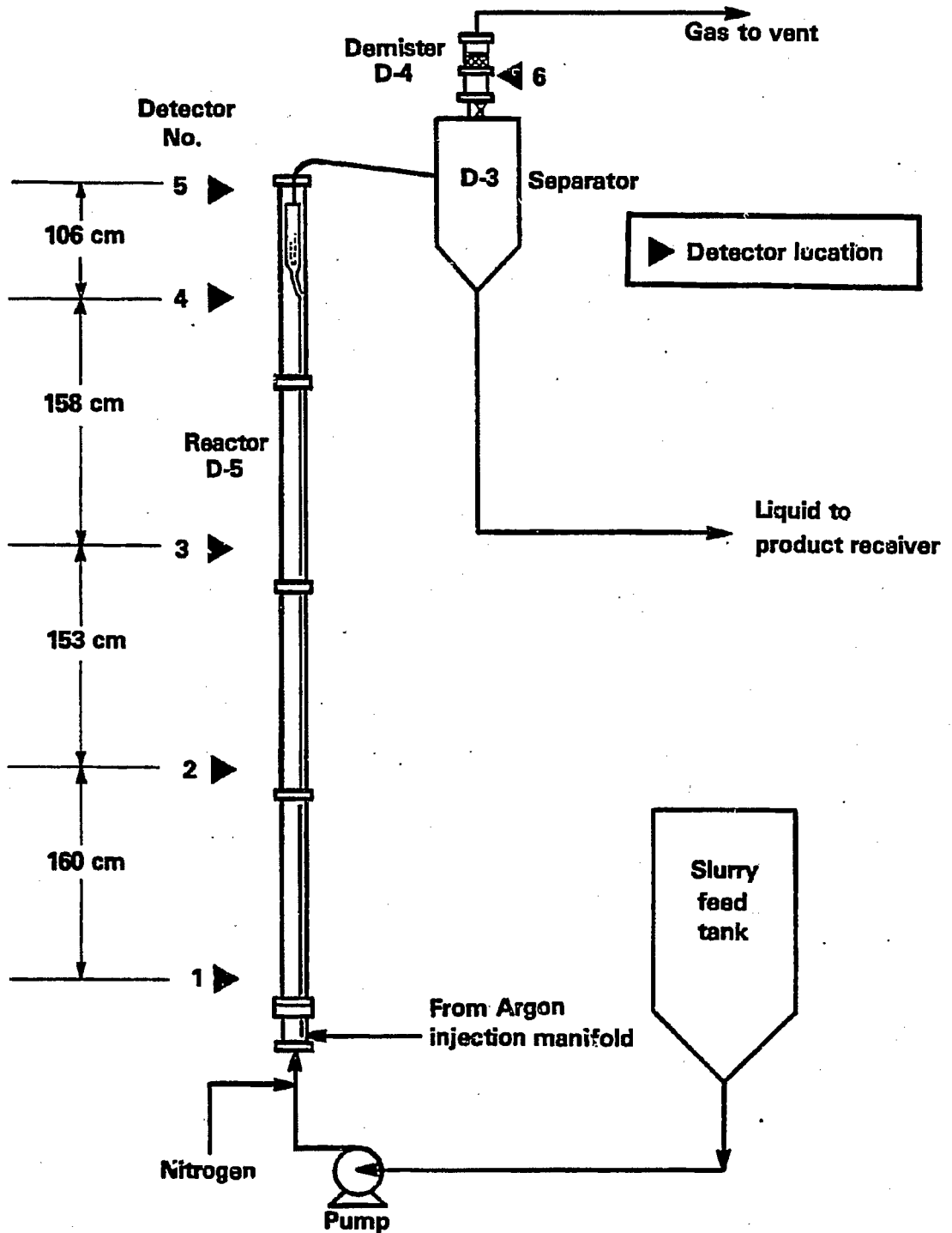


Figure 2

Tracer results with 0 vol % coal char

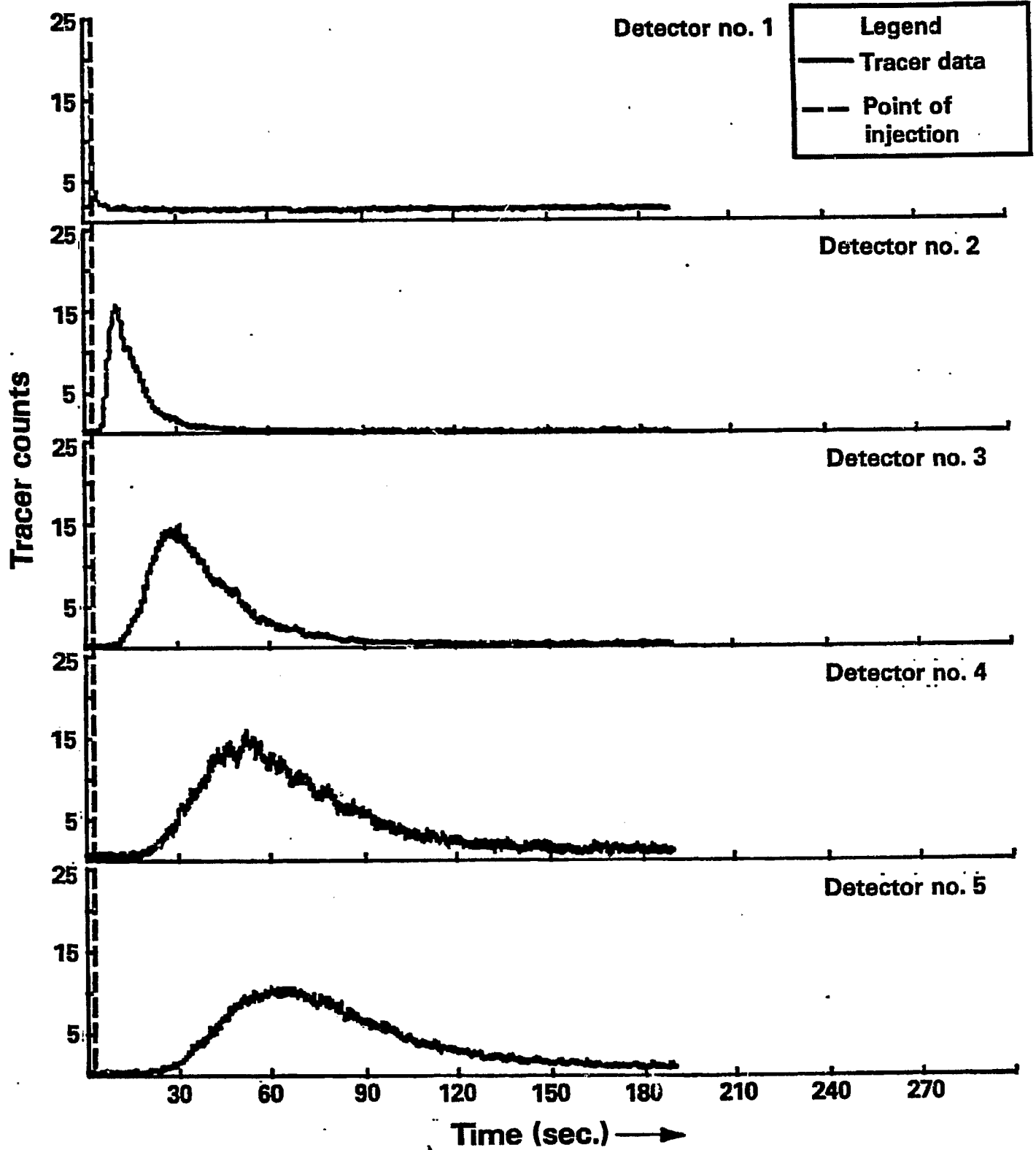


Figure 3

Tracer results with 15.5 vol % coal char

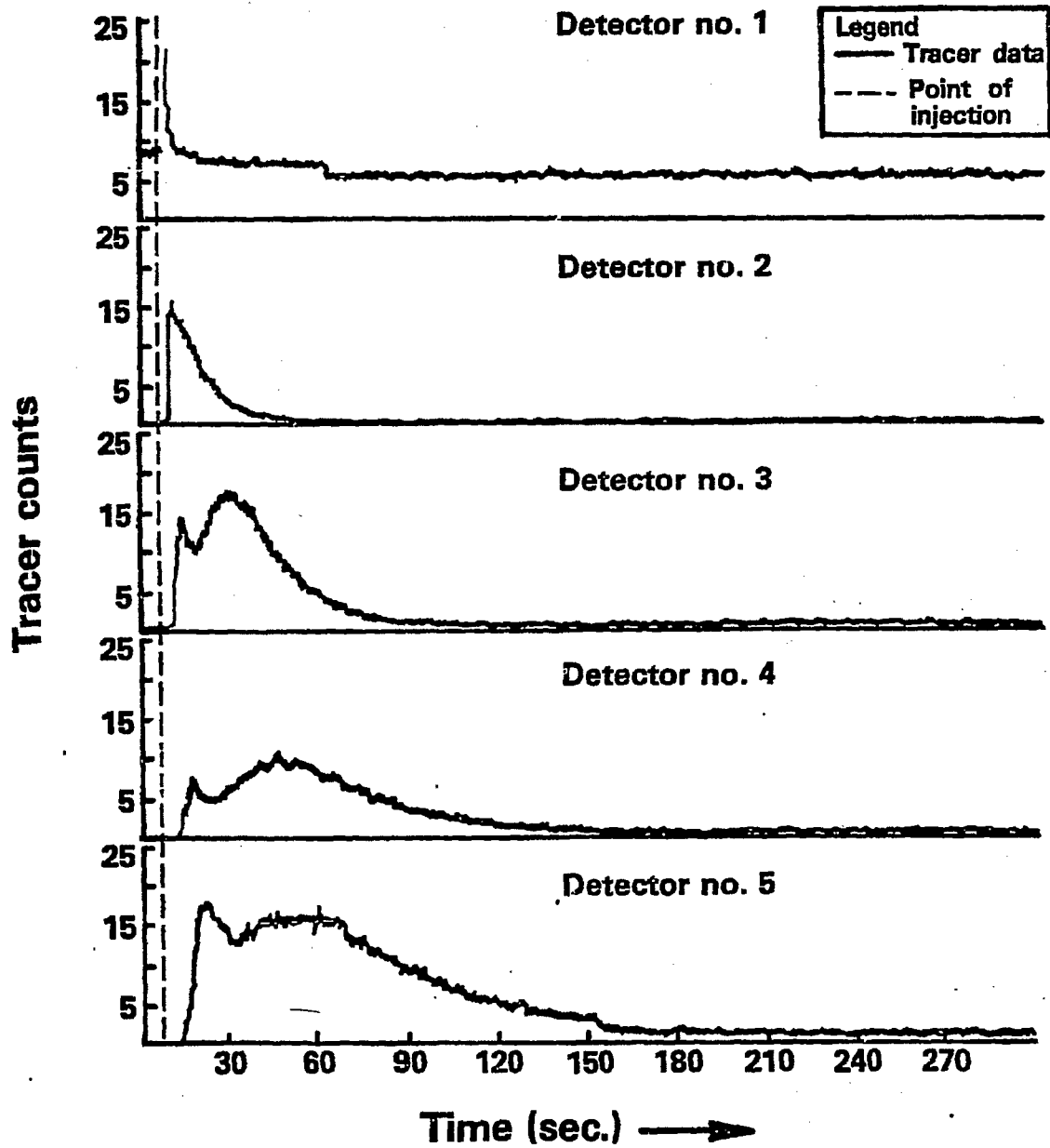


Figure 4
Gas mixing model

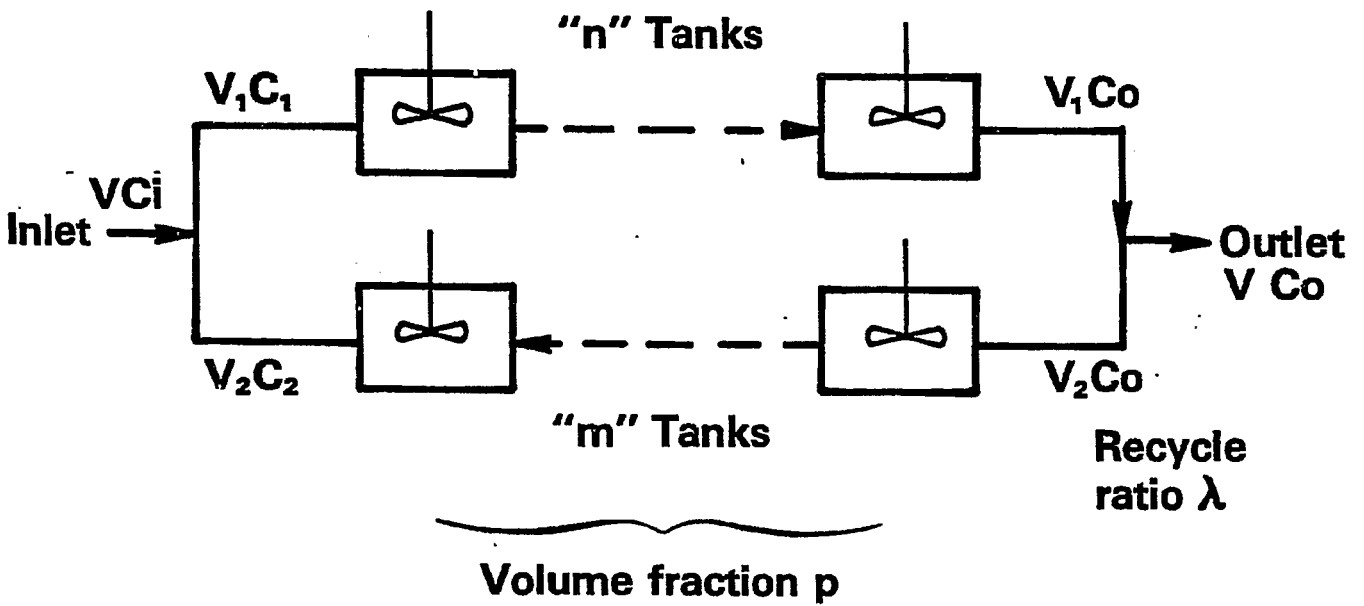


Figure 5

FLOW DIAGRAM FOR
COMPUTATION PROCEDURE

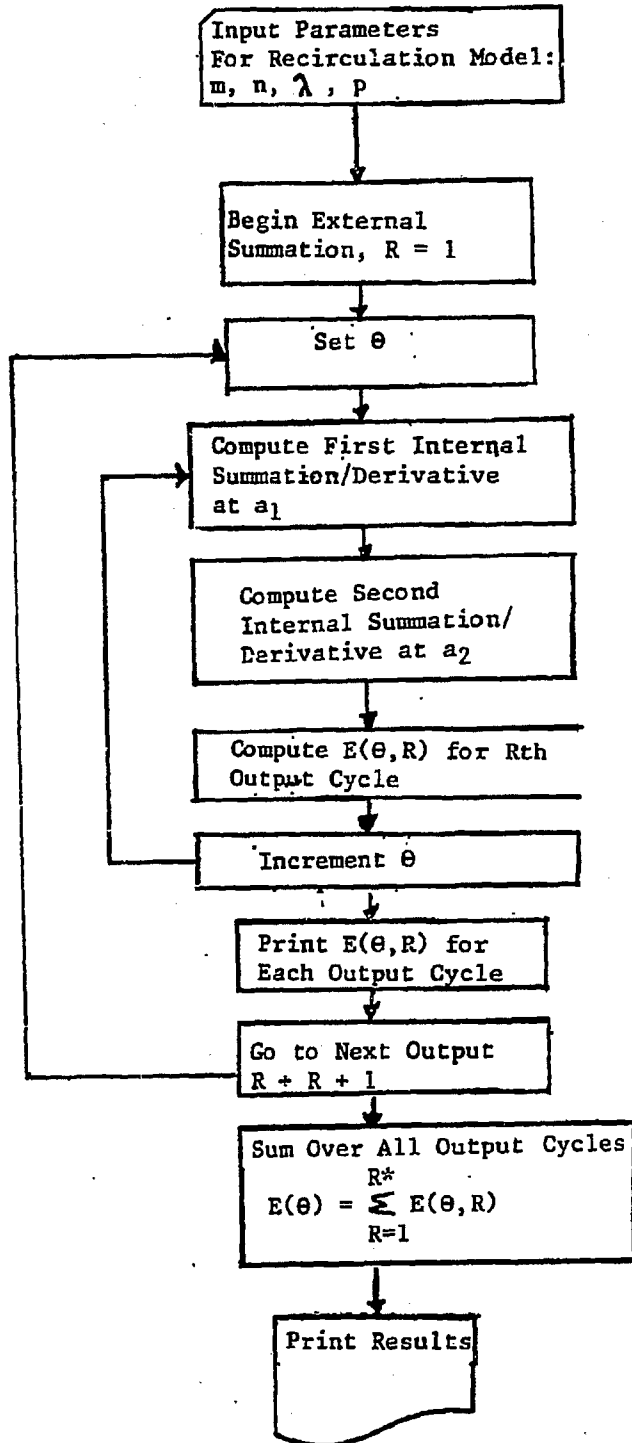


Figure 6

Typical response curves based on the proposed model

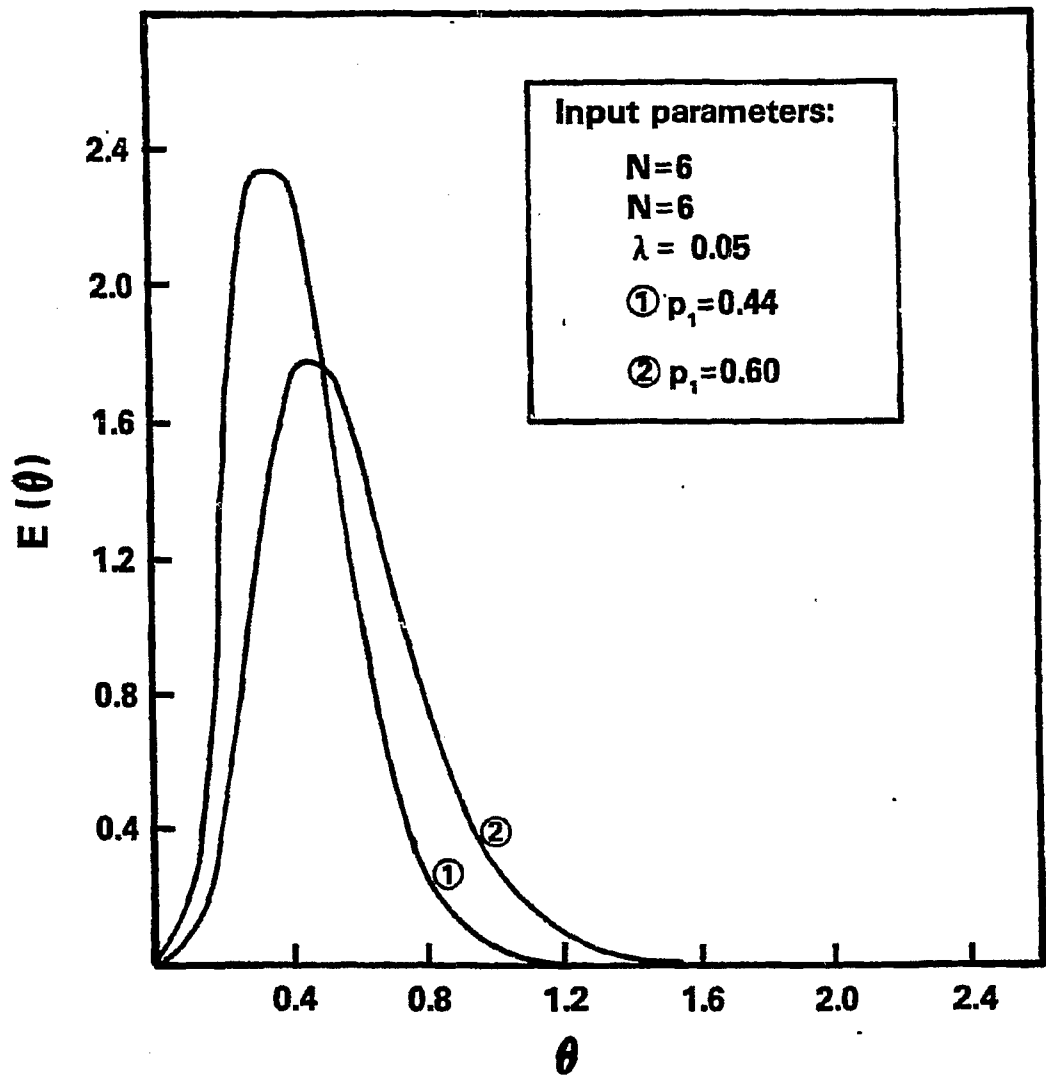


Figure 7

Typical response curves based on the proposed model

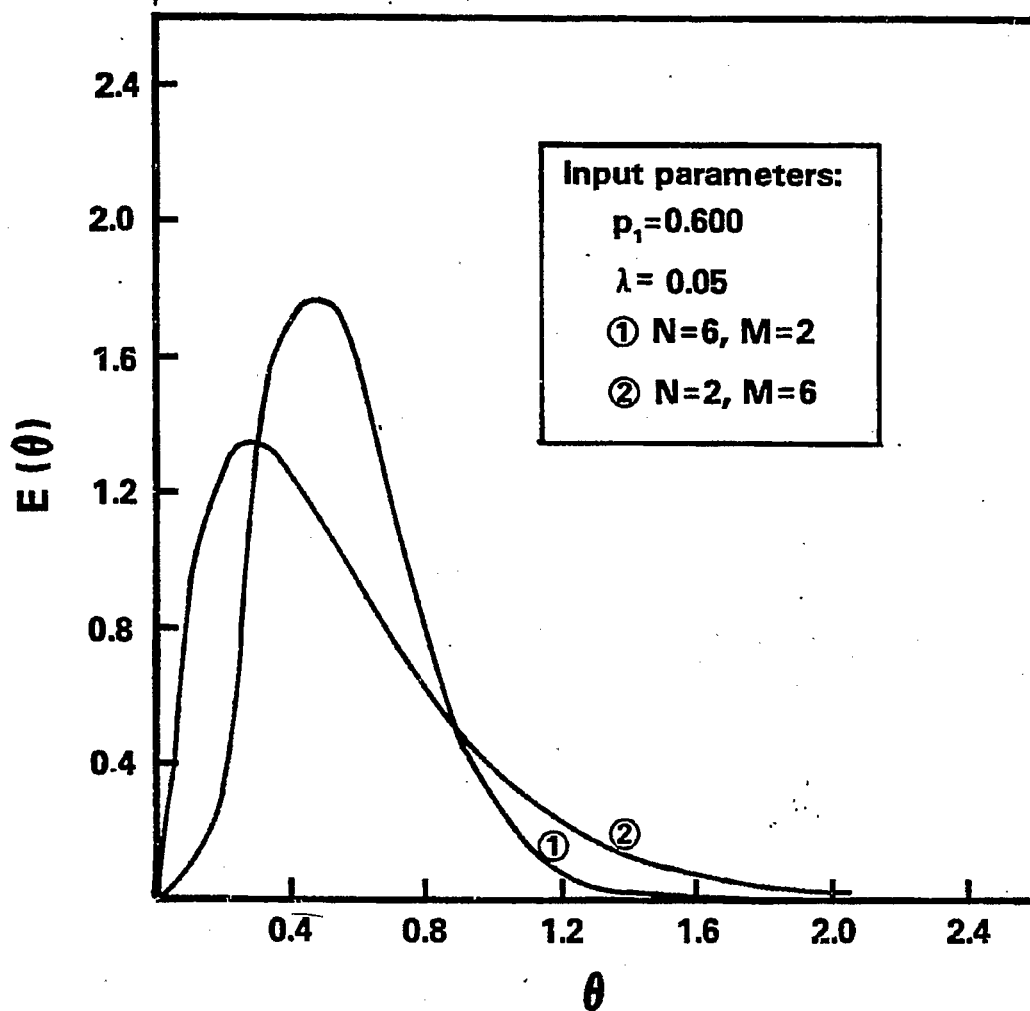


Figure 8

Comparison of gas mixing model with experiments:
Kerosene/catalyst/no fines

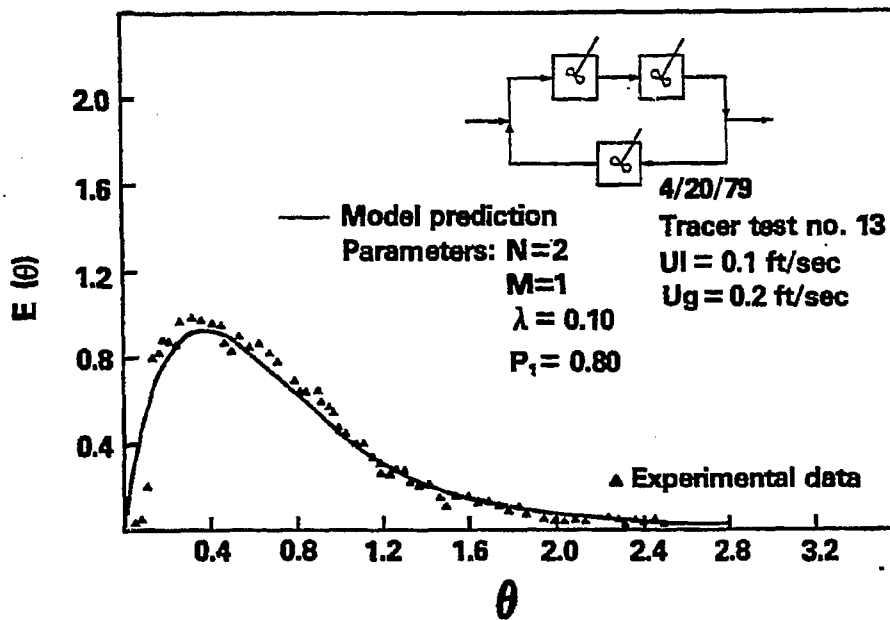
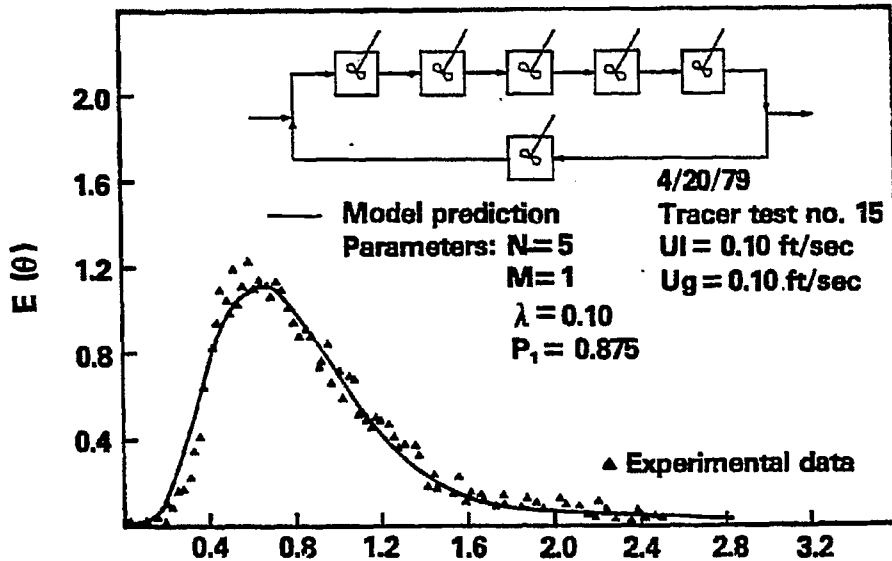


Figure 9

Comparison of gas mixing model with experiments:
Kerosene/catalyst/15.5 vol % coal fines

